H_2 doubly-excited-state assignment from the determination of the orbital state of the $H^*(n=3)$ photodissociation fragments

M. Glass-Maujean
Laboratoire Kastler Brossel, Université Pierre et Marie Curie, 4 Place Jussieu, 75252 Paris Cedex 05, France and Laboratoire pour l'Utilisation du Rayonnement Electromagnétique, Laboratoire CNRS/CEA/MEN, 91405 Orsay Cedex, France

H. Frohlich
Laboratoire des Collisions Atomiques et Moléculaires, Université Paris Sud, 91405 Orsay Cedex, France and Laboratoire pour l'Utilisation du Rayonnement Electromagnétique, Laboratoire CNRS/CEA/MEN, 91405 Orsay Cedex, France

P. Martin
Laboratoire pour l'Utilisation du Rayonnement Electromagnétique, Laboratoire CNRS/CEA/MEN, 91405 Orsay Cedex, France
(Received 10 January 1995; revised manuscript received 24 July 1995)

The photodissociation of doubly excited H_2 has been experimentally investigated. Using the pulsed character of the incident synchrotron radiation, the time analysis of the atomic fragment fluorescence Balmer-α (H_α) decay was used for identification of the fragments. The measured branching ratios of the $H(3l)$ fragments at a given photon energy contain information about the dynamic behavior of the photodissociation. The states of the first Rydberg series, $Q_1(2p\sigma,nl\lambda)$, dissociating into $H(1S)+H(n=3)$ lead almost to $H(1S)+H(3S)$ fragments; the state involved can be identified from the correlation diagram as the $(2p\sigma_u,4d\sigma_g)$ configuration. The photodissociating states of the second Rydberg series, $Q_2(2p\pi,nl\lambda)$, lead to $H(2p)+H(n=3)$, the $H(n=3)$ fragments being a mixture of $H(3S)$ and $H(3D)$ in a ratio of about 2:1. In order to identify the relevant Q_2 state, the energy ordering in the manifold of the molecular states dissociating into $H^*(n=2)$ and $H^*(n=3)$ has been established by calculating the whole dipole-dipole long-range interaction.

PACS number(s): 33.80.Gj, 34.50.Gb

I. INTRODUCTION

The vertical excitation energies of doubly excited states of H_2 (H_2**) exceed 23 eV, far above the ionization threshold (15.4 eV). Thus, dissociation of H_2** into neutral fragments competes with autoionization. These states belong mainly to two Rydberg series, labeled Q_1 and Q_2, with, respectively [1], $(2p\sigma_u,nl\lambda_g)$ and $(2p\pi_u,nl\lambda_g)$ united-atom orbital configurations. The potential-energy curves of some of the doubly excited states of H_2 are shown in Fig. 1. The Q_1 states are correlated to $(\sigma_u 1s,\lambda_g n'l')$ at a large distance corresponding either to $H(1S)+H^*(n'l')$ or to $H^+ + H^-(1s,n'l')$ [2]. For all these states, the dissociation competes with the formation of H_2^+ and H^+ ions.

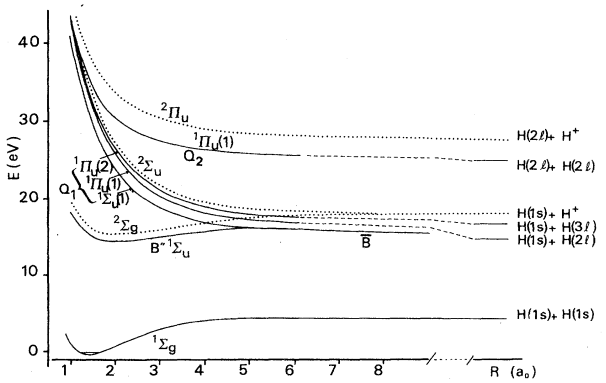

FIG. 1. Potential-energy curves of the H_2 states (full lines) and H_2^+ states (dotted lines) [1].

Such dissociation yields fast atoms ($v \geq 20$ km/s), which have been observed many years ago by electron impact. By a time-of-flight technique, Leventhal, Robiscoe, and Lea [3] were first to put into evidence fast $H(2S)$ atoms and to suggest that doubly excited molecular states were responsible for them. Misakian and Zorn [4] then identified the lowest $^1\Pi_u(2p\pi_u 2s\sigma_g)$ among the Q_2 manifold as the main parent molecular state, the dissociation of which was calculated by Hazi and Wiemers [5]. Spezeski, Kalman, and McIntyre [6] later on settled the importance of the Q_1 states besides the Q_2 previously assigned. Fast long-lived fragments were then observed by translational spectroscopy [7]. Later on, fast short-lived fragments were studied by the Doppler profile analysis of Balmer lines [8,9].

Photoexcitation of the doubly excited states from the ground state occurs through a forbidden dipole transition, allowed only by the two-electron correlations. Despite the very low values of the absorption cross section, photodissociation could be observed leading to $H(n=2)$ [10,11], $H(n=3)$, and $H(n=4)$ atoms [12]. It has been recognized that some of those states undergo dissociation as the major deexcitation channel [4,5,10]. The goal of the present work is to determine the branching ratio of the $H(n=3)$ orbital angular momentum photofragments and to assign the configuration of the parent molecular states that leads to these atomic states.

II. EXPERIMENTAL SETUP

Monochromatized synchrotron radiation ($300<\lambda<500$ Å) was used to excite H_2 molecules contained in a differen-

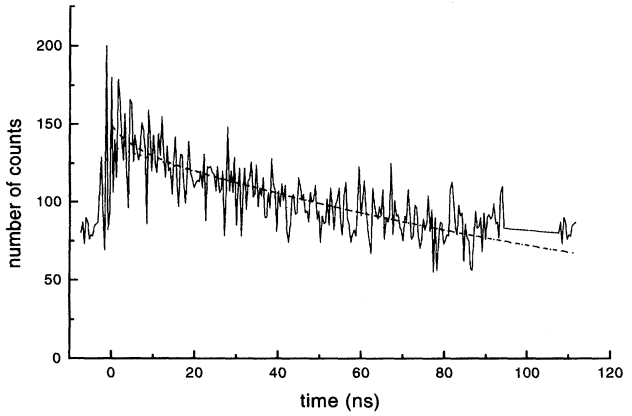

FIG. 2. H_α decay after excitation of H_2 at $\lambda = 400$ Å: experimental and best fit (dashed line) corresponding to $5 \pm 10\%$ of $3P$ and 95% of $3S$ state. The dotted line corresponds to the best fit for a pure $3S$ excitation.

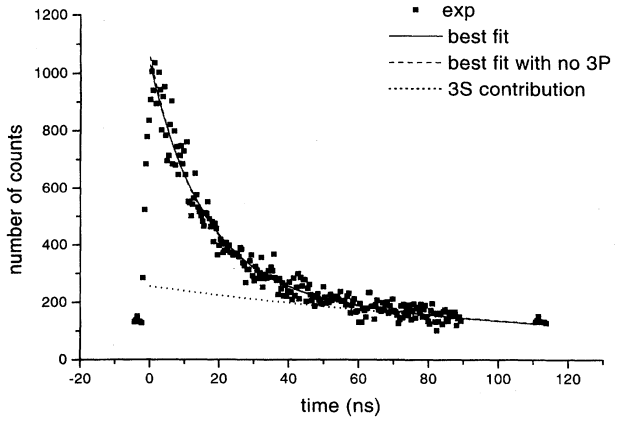

FIG. 3. H_α decay after excitation of H_2 at $\lambda = 346$ Å: experimental and best fit (dashed line) corresponding to $58 \pm 2\%$ of $3S$, $42 \pm 2\%$ of $3D$, and $0 \pm 10\%$ of $3P$. The dotted line represents the $3S$ contribution.

tially pumped cell maintained at a constant pressure of the order of 5 mT. The $H_\alpha(n=3 \rightarrow n=2)$ fluorescence of the atomic fragments was time-analyzed [13].

A 3-m normal-incidence monochromator (Balzers) equipped with a Pt-coated, 2200 lines per mm holographic grating was used in the first order. The spectral bandwidth used was about 2 Å.

The Balmer-α fluorescence was detected at right angles from the incident light, collected by a Plexiglass light pipe, filtered with a red-colored Wratten filter, and detected by a refrigerated red-sensitive photomultiplier (RTC XP2254B), using a traditional single-photon counting technique. When operating with two positron bunches in the storage ring, the delay between two consecutive synchrotron light pulses was 115 ns. The analysis period was 100 ns digitalized by 256 channels. The decay of the Balmer-α emission was obtained by substraction of the signals recorded with and without hydrogen gas present in the chamber, in order to eliminate the residual gas (N_2) contribution. Data with backgrounds that could not be reduced by this procedure had been rejected. No pressure dependence of the signal was observed below 6 mT.

III. RESULTS

The $H(n=3)$ states have quite different lifetimes (τ_L): 158, 15.5, and 5.3 ns [14] for $3S$, $3D$, and $3P$, respectively. The experimental decay curves were fitted by a function defined as the sum of three exponentials with these known lifetimes τ_L. The amplitudes of the exponentials were constrained to be non-negative (Figs. 2 and 3). The points displayed at negative t values represent neither the asymptote of the signal nor the background but are due to the piling up of the decay signal at

$$t = T_R - |t|, \tag{1}$$

T_R being the synchrotron repetition period. This is shown in Fig. 2, where these negative time points are placed at their real time positions. As the period is 115 ns and the time-analyzed delay only 100 ns, a small portion of the delay spectrum is not measured, corresponding to the flat part in Fig. 2.

The $3S$, $3D$, and $3P$ contributions were deduced from the integration of these components over the repetition period T_R:

$$\sigma(3L) = \gamma_L \int_0^{T_R} n_L(t)dt = \gamma_L n_L(0) \int_0^{T_R} e^{-t/\tau_L} dt$$

$$= \gamma_L n_L(0) \tau_L (1 - e^{-T_R \tau_L}). \tag{2}$$

To obtain the $3S$, $3D$, and $3P$ populations we had to take into account that the $3S$ and $3D$ states radiate only through H_α line ($\gamma_S = \gamma_D = 1$), whereas the $3P$ state radiates with 88% relative probability through the here unobserved L_β channel ($\gamma_P = 0,12$) [14]. The relative populations of the $3S$, $3D$, and $3P$ states have been determined for various excitation wavelengths ranging from 340 to 407 Å (36.5 to 30.5 eV) (Fig. 3).

For incident wavelengths greater than 370 Å, the decay curves exhibit the same behavior as that displayed in Fig. 2. The dashed line represents the best fit; it leads to $95 \pm 5\%$ of $3S$ fragments, $5 \pm 10\%$ of $3P$ fragments, and $0 \pm 4\%$ of $3D$ (the quoted errors are twice the standard deviation). The fit with a single exponential of width $\tau_s = 158$ ns is displayed by a dotted line. It corresponds to a dissociation into pure $H(3S)$ fragments.

In the 340–360 Å excitation range, both $3S$ and $3D$ fragments are present (Fig. 3). As shown there, at short decay time, the two fits, with and without $3P$ contribution, can hardly be distinguished. Thus, the presence of $3P$ fragments cannot be ascertained, but a value of $5 \pm 10\%$ of the $3S+3D$ population can be deduced. The measured $3D$ to $(3S+3D)$ relative population is observed to increase with energy, as shown in Fig. 4(a).

The energy variation of the branching ratio $3D$ to $(3S+3D)$ can be put into relation with the total photodissociation cross section (Ref. [12]) and displayed [Fig. 4(b)]. If the $3D$ to $(3S+3D)$ branching ratio of the Q_2 fragments is taken as constant over the whole spectral range, the $3D$ to

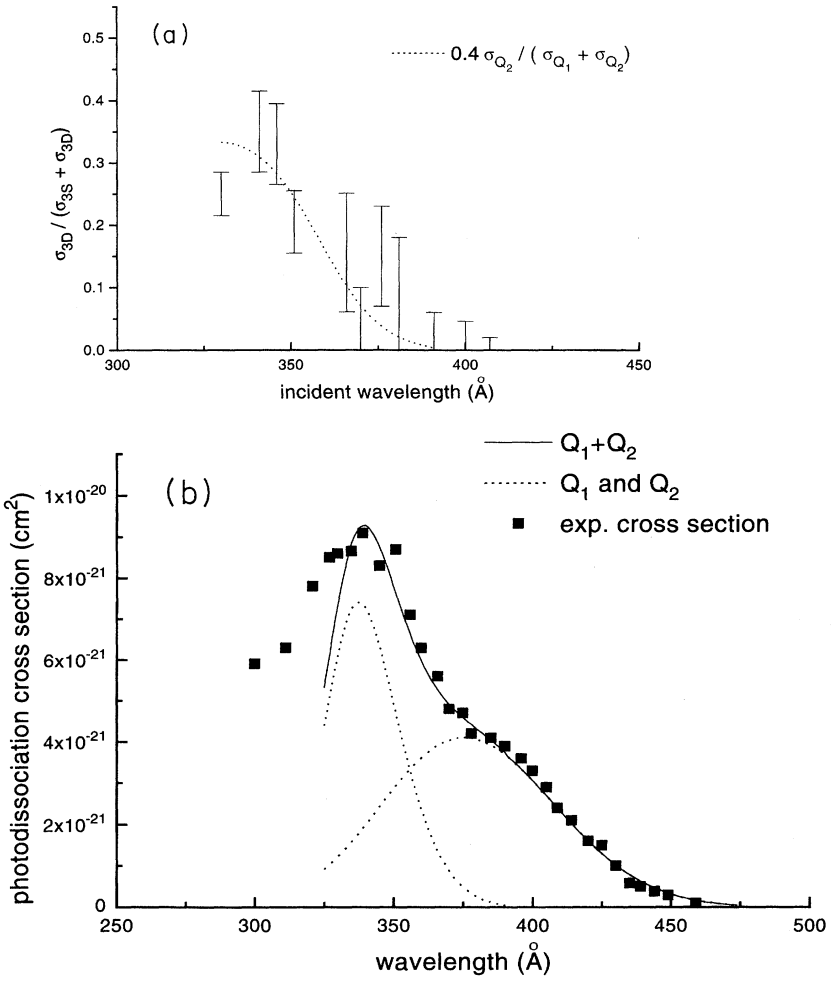

FIG. 4. (a) The $\sigma_{3D}/(\sigma_{3S}+\sigma_{3D})$ branching ratios (error bars) as a function of the excitation wavelength displayed with the weighted Q_2 relative cross section computed from the data of (b). (b) The experimental $\sigma_{n=3}$ data (solid squares) are superimposed to a theoretical curve (full line). The dotted lines represents the Q_1 and Q_2 contributions to the $\sigma_{n=3}$ theoretical curve (from Ref. [12]).

the total $(3S+3D)$ population has to be proportional to the relative cross section $\sigma_{Q2}/(\sigma_{Q1}+\sigma_{Q2})$ previously determined in Ref. [12]. The agreement between the two ratio variations is displayed in Fig. 4(a) (dotted line), leading to the determination of the constant value

$$\sigma(3D)/[\sigma(3S)+\sigma(3D)]=0.4\pm0.1$$

for the Q_2 branching ratio over the investigated spectral range, i.e., typically two $3S$ fragments for one $3D$.

IV. DISCUSSION

For excitation wavelengths between 407 to 380 Å ($E<32$ eV) the H($n=3$) fragments originate from the dissociation of Q_1 doubly excitation states [12], while for shorter wavelengths (340 to 380 Å) both Q_1 and Q_2 states contribute. From the H_α emission cross-section curve, it has been established [12] that the dissociating Q_1 state corresponds to a Rydberg state of the H_2^+ $(2p\sigma_u\,^2\Sigma_u)$ ion core with a $4l\lambda_g$ orbital and that the dissociating Q_2 state corresponds to a Rydberg state of the H_2^+ $(2p\pi_u\,^2\Pi_u)$ ion core with a $3l\lambda_g$ orbital $[Q_2\,^1\Pi_u(2)\ (2p\pi_u,3d\sigma_g)]$.

A. Q_1 state

The overwhelming occurrence of the $3S$ fragments in this case implies a single $\Lambda=0$ molecular state for the parent-excited molecule. Among the possible Q_1 states of $^1\Sigma_u^+$ symmetry satisfying the above configuration, there is the $(2p\sigma_u,4s\sigma_g)^2\Sigma_u$ (4) or the $(2p\sigma_u,4d\sigma_g)^1\Sigma_u$ (5) state.

The Q_1 states $2p\sigma_u,nl\lambda_g$ and the singly excited state $(1s\sigma_g,nl\lambda_u)$ are both correlated to $1sm=0$, $n'l'm'=\lambda$ at large distance, with both atomic and ionic character [15] giving covalent $H(1s)+H(nl)$ and higher-lying ionic $H^+ + H^-(1s,nl)$ limits. A pure adiabatic description would link the ionic limit to the Q_1 states and the covalent one to the singly excited states. However, the observation of $H^*(n=3)$ fragments proves that the Q_1 dissociation is not adiabatic.

The kinetic energy of Q_1 dissociation fragments exceeds 15 eV. A diabatic behavior is thus expected between the Q_1 states and the crossed singly excited states, whereas the small energy gap between two neighboring Q_1 states may favor an adiabatic behavior inside the Q_1 set.

Following this rationale we determined the adiabatic correlation diagram for the $^1\Sigma_u$ Q_1 set. The relative energy position of the states in the united-atom limit reflects the l dependence of the quantum defect for penetrating orbitals. At

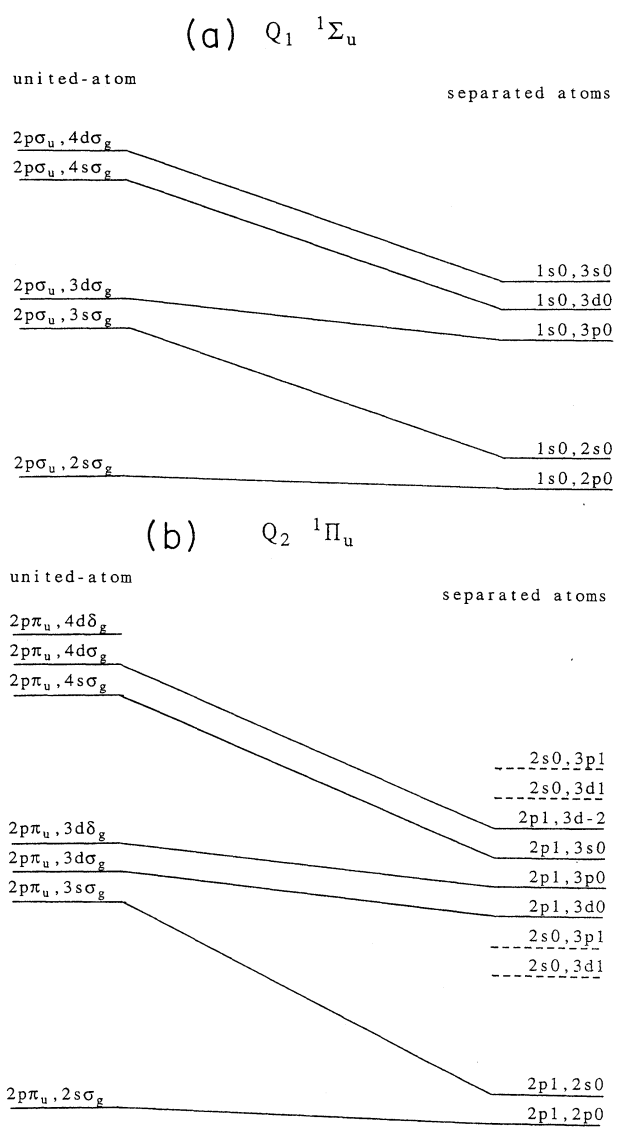

FIG. 5. (a) Adiabatic correlation diagram for the $Q_1\,^1\Sigma_u^+$ states (see text). (b) Adiabatic correlation diagram for the $Q_2\,^1\Pi_u$ states (see text).

very large distances, the ordering of the levels depends on the long-range interactions between the excited atom and the atom in its ground state [16]. The potential curves for the long-range interaction between an H($1s$) and an H ($3lm_l=0$) atom have been calculated [16]. For the $^1\Sigma_u^+$ symmetry, the order of increasing energy is ($1s0,3p0$), ($1s0,3d0$), followed by ($1s0,3s0$). The $(1s0,3p0)\,^1\Sigma_u$ configuration gives an attractive dipole-dipole potential, the ($1s0,3d0$) an attractive dipole-quadrupole potential, and the ($1s0,3s0$) only a dipole-dipole induced term. The adiabatic correlation diagram for the $^1\Sigma_u^+$ Q_1 set is presented in Fig. 5(a). The adiabatic correlation diagram shows that the $1S+3S$ limit correlates to $(2p\sigma_u,4d\sigma_g)$ in agreement with the previously assigned $4l\lambda_g$ orbital.

B. Q_2 state

The Q_2 states involved in the dissociation leading to H($2P$)+H($3D$ and $3S$) fragments have to be of $^1\Pi_u$ symmetry. As already discussed, the dissociation is expected to be diabatic except inside the Q_2 set. To build up the adiabatic correlation diagram, we have to sort the $^1\Pi_u$ states at a large internuclear distance by computing the long-range potential curves for the ($2pm_l=1$, $3lm_l'=0,-2$) configurations. This is shown in the Appendix.

Eight different $^1\Pi_u$ ($n=2,n=3$) configurations are degenerate at infinity. The dipole-dipole interaction mixes them into two groups; among these eight states, the $Q_2\,^1\Pi_u$ states represent only four. The diagonalization of the interaction matrix leads to the ordering of states that are no longer ($2lm_l,3l'm_l'$) states. Taking the main configuration for each of them as a label for the states and rejecting the non-Q_2 states, we obtained the adiabatic correlation diagram of Fig. 5(b).

The state with the ($2p1,3s0$) main configuration can be associated with the calculated fragment composition of 59% S, 40% D, and 2% P, which agrees with the observed values. This state is correlated to the $(2p\pi_u,4s\sigma_g)$ $Q_2\,^1\Pi_u$ state. According to the calculations of Guberman [1] its effective quantum number is expected to be $n^*_{Q_2}=3.9$, in disagreement with the previous assignment [12]. In addition, we can show that none of the superpositions of the available states is able to reproduce the observed fragmentation ratios. As in the case of the Q_1 state, the observed H($n=2$)+H($n=3$) photodissociation is dominated by a single Q_2 state.

V. CONCLUSION

We measured the branching ratios of the orbital angular momentum states of the H($n=3$) fragments following the photodissociation of doubly excited states of H_2 and their relative occurrence, depending on the excitation energy. The observation of $3S$ fragments from the Q_1 dissociation invalidates the previous assignment at the $^1\Pi_u(2)$ state, deduced from a cross-section curve fit [10]. To assign the dissociative states, we considered the adiabatic correlation diagrams, based on the long-range interaction potentials, assuming a diabatic behavior between the Q_1 or Q_2 states and the singly excited configurations and assuming an adiabatic one inside the states of the same set Q_1 or Q_2. We have calculated the dipole-dipole interaction between the H*($n=2$)+H*($n=3$) atoms. From this interaction matrix we were able to calculate the eigenvalues and eigenfunctions. The observed Q_1 dissociating state can be assigned to the $(2p\pi_u,4d\sigma_g)\,^1\Sigma_u$ state. The Q_2 dissociating state is the $(2p\pi_u,4s\sigma_g)\,^1\Pi_u$ state, with an adiabatic limit being a state superposition of H*($2P$)+H*($3S$) and H*($2P$)+H*($3D$) fragments.

APPENDIX: CALCULATION OF THE INTERACTION BETWEEN H*($N=2$) AND H*($N=3$) ATOMS AT LARGE SEPARATIONS

The long-range interaction between atoms had been treated by Fontana in 1961 giving general formulas [17]. His

TABLE I. $^1\Sigma$ dipole-dipole interaction matrix on the unperturbed separated atom basis set. The numbers (in atomic units) have to be divided by R^3.

		$^1\Sigma_u^+, {}^3\Sigma_g^+$		
	$\|2s0,3p0,+\rangle$	$\|2p0,3s0,+\rangle$	$\|2p0,3d0,+\rangle$	$\|2p1,3d-1,+,+\rangle$
$\|2s0,3p0,+\rangle$	−6.262 062	−44.090 817	−39.436 025	−19.091 884
$\|2p0,3s0,+\rangle$	−44.090 817	−0.587 068	−2.656 768	−1.626 931
$\|2p0,3d0,+\rangle$	−39.436 025	−2.656 768	−12.023 160	−9.017 370
$\|2p1,3d-1,+,+\rangle$	−19.091 884	−1.626 931	−9.017 370	−9.017 370
		$^1\Sigma_u^+, {}^3\Sigma_g^+$		
	$\|2s0,3s0,-\rangle$	$\|2s0,3d0,-\rangle$	$\|2p0,3p0,-\rangle$	$\|2p1,3p-1,-,+\rangle$
$\|2s0,3s0,-\rangle$	0.000 000	0.000 000	−42.173 460	−29.821 140
$\|2s0,3d0,-\rangle$	0.000 000	0.000 000	−22.499 947	−13.778 348
$\|2p0,3p0,-\rangle$	−42.173 460	−22.499 947	0.000 000	0.000 000
$\|2p1,3p-1,-,+\rangle$	−29.821 140	−13.778 348	0.000 000	0.000 000
		$^1\Sigma_g^+, {}^3\Sigma_u^+$		
	$\|2s0,3p0,-\rangle$	$\|2p0,3s0,-\rangle$	$\|2p0,3d0,-\rangle$	$\|2p1,3d-1,-,+\rangle$
$\|2s0,3p0,-\rangle$	6.262 062	44.090 817	39.436 025	19.091 884
$\|2p0,3s0,-\rangle$	44.090 817	0.587 068	2.656 768	1.626 931
$\|2p0,3d0,-\rangle$	39.436 025	2.656 768	12.023 160	9.017 370
$\|2p1,3d-1,-,+\rangle$	19.091 884	1.626 931	9.017 370	9.017 370
		$^1\Sigma_g^+, {}^3\Sigma_u^+$		
	$\|2s0,3s0,+\rangle$	$\|2s0,3d0,+\rangle$	$\|2p0,3p0,+\rangle$	$\|2p1,3p-1,+,+\rangle$
$\|2s0,3s0,+\rangle$	0.000 000	0.000 000	−46.008 174	−32.532 692
$\|2s0,3d0,+\rangle$	0.000 000	0.000 000	−39.853 883	−24.405 420
$\|2p0,3p0,+\rangle$	−46.008 174	−39.853 883	0.000 000	0.000 000
$\|2p1,3p-1,+,+\rangle$	−32.532 692	−24.405 420	0.000 000	0.000 000

approach had been previously used to investigate the long-range interaction between hydrogen atoms, one of which was excited [16,18] or both excited in the $n=2$ states [19]. We need to extend this calculation to the $H^*(n=2)+H^*(n=3)$ level set.

Neglecting the fine and hyperfine structures, the unperturbed wave function is a product of hydrogen atom eigenfunctions,

$$|n_1 l_1 m_1, n_2 l_2 m_2\rangle = \varphi_{n_1 l_1 m_1}(r_{1a})\varphi_{n_2 l_2 m_2}(r_{2b}), \quad \text{(A1)}$$

where the φ_{nlm} are the ordinary hydrogen-atom wave functions with atomic quantum numbers nlm. The r_{1a} is the radius vector of the electron 1 with respect to the nucleus a (and similar for r_{2b}); the functions (2) correspond to $\Lambda = m_1 + m_2$, the total orbital angular momentum along the internuclear axis, which is an exact quantum number for the diatomic molecule in the Born-Oppenheimer approximation. The functions (1) correspond at infinite internuclear distance to the energy

$$E_0 = -\tfrac{1}{2}(n_1^{-2} + n_2^{-2}) \quad \text{(in atomic units)}. \quad \text{(A2)}$$

According to Fontana, the electrostatic interaction energy can be expanded as a sum of coupling terms between multipole moments written in an irreducible tensor basis set. The interaction matrix elements V_s can be expressed in the form (Refs. [16] and [19])

$$V_S = \langle n_1 l_1 m_1, n_2 l_2 m_2 | V | n_1' l_1' m_1', n_2' l_2' m_2' \rangle = \sum_{l_a, l_b, \mu} (-1)^{l_b + m_1' m_2'} \frac{e}{R^{l_a + l_b + 1}} (l_a + l_b)! \langle n_1 l_1 | r_{1a}^{l_a} | n_1' l_1' \rangle \langle n_2 l_2 | r_{2b}^{l_b} | n_2' l_2' \rangle$$
$$\times [(2l_1+1)(2l_1'+1)(2l_2+1)(2l_2'+1)]^{1/2} [(l_a-\mu)!(l_a+\mu)!(l_b-\mu)!(l_b+\mu)!]^{-1/2}$$
$$\times \begin{pmatrix} l_1 & l_a & l_1' \\ 0 & 0 & 0 \end{pmatrix} \begin{pmatrix} l_2 & l_b & l_2' \\ 0 & 0 & 0 \end{pmatrix} \begin{pmatrix} l_1' & l_a & l_1 \\ -m_1' & -\mu & m_1 \end{pmatrix} \begin{pmatrix} l_2' & l_b & l_2' \\ -m_2' & \mu & m_2 \end{pmatrix}, \quad \text{(A3)}$$

TABLE II. Same as Table I for the $^1\Pi$ states.

	$^1\Pi_u, ^3\Pi_g$				
	$\|2p1,3s0,+\rangle$	$\|2p1,3d0,+\rangle$	$\|2p0,3d1,+\rangle$	$\|2p-1,3d2,+\rangle$	$\|2s0,3p1,+\rangle$
$\|2p1,3s0,+\rangle$	0.293 534	−1.992 576	−2.300 829	−1.626 932	22.045 408
$\|2p1,3d0,+\rangle$	−1.992 576	1.502 895	−10.412 362	1.840 663	−7.794 229
$\|2p0,3d1,+\rangle$	−2.300 829	−10.412 362	4.508 685	0.000 000	27.000 000
$\|2p-1,3d2,+\rangle$	−1.626 932	1.840 663	0.000 000	9.017 370	−19.091 883
$\|2s0,3p1,+\rangle$	22.045 408	−7.794 229	27.000 000	−19.091 883	3.131 031

	$^1\Pi_u, ^3\Pi_g$		
	$\|2s0,3d1,-\rangle$	$\|2p0,3p1,-\rangle$	$\|2p1,3p0,-\rangle$
$\|2s0,3d1,-\rangle$	0.000 000	37.909.836	24.590 774
$\|2p0,3p1,-\rangle$	37.909 836	0.000 000	0.000 000
$\|2p1,3d0,-\rangle$	24.590 774	0.000 000	0.000 000

	$^1\Pi_g, ^3\Pi_u$				
	$\|2p1,3s0,-\rangle$	$\|2p1,3d0,-\rangle$	$\|2p0,3d1,-\rangle$	$\|2p-1,3d2,-\rangle$	$\|2s0,3p1,-\rangle$
$\|2p1,3s0,-\rangle$	−0.293 534	1.992 576	2.300 829	1.626 932	−22.045 408
$\|2p1,3d0,-\rangle$	1.992 576	−1.502 895	10.412 362	−1.840 663	7.794 229
$\|2p0,3d1,-\rangle$	2.300 829	10.412 362	−4.508 685	0.000 000	−27.000 000
$\|2p-1,3d2,-\rangle$	1.626 932	−1.840 663	0.000 000	−9.017 370	19.091 883
$\|2s0,3p1,-\rangle$	−22.045 408	7.794 229	−27.000 000	19.091 883	−3.131 031

	$^1\Pi_g, ^3\Pi_u$		
	$\|2s0,3d1,+\rangle$	$\|2p0,3p1,+\rangle$	$\|2p1,3p0,+\rangle$
$\|2s0,3d1,+\rangle$	0.000 000	30.395 361	9.561 825
$\|2p0,3p1,+\rangle$	30.395 361	0.000 000	0.000 000
$\|2p1,3d0,+\rangle$	9.561 825	0.000 000	0.000 000

TABLE III. Same as Table I for the $^1\Delta$ and $^1\Phi$ states.

	$^1\Delta_u, ^3\Delta_g$			
	$\|2p1,3d1,+\rangle$	$\|2p0,3d2,+\rangle$	$\|2s0,3d2,-\rangle$	$\|2p1,3p1,-\rangle$
$\|2p1,3d1,+\rangle$	−9.017 370	6.376 243	0.000 000	0.000 000
$\|2p0,3d2,+\rangle$	6.376 243	0.000 000	0.000 000	0.000 000
$\|2s0,3d2,-\rangle$	0.000 000	0.000 000	0.000 000	13.778 348
$\|2p1,3p2,-\rangle$	0.000 000	0.000 000	13.778 348	0.000 000

	$^1\Delta_g, ^3\Delta_u$			
	$\|2p1,3d1,-\rangle$	$\|2p0,3d2,-\rangle$	$\|2s0,3d2,+\rangle$	$\|2p1,3p1,+\rangle$
$\|2p1,3d1,-\rangle$	9.017 370	−6.376 243	0.000 000	0.000 000
$\|2p0,3d2,-\rangle$	−6.376 243	0.000 000	0.000 000	0.000 000
$\|2s0,3d2,+\rangle$	0.000 000	0.000 000	0.000 000	24.405 421
$\|2p1,3p2,+\rangle$	0.000 000	0.000 000	24.405 421	0.000 000

	$^1\Phi_u, ^3\Phi_g$
	$\|2p1,3d2,+\rangle$
$\|2p1,3d2,+\rangle$	9.017 370

	$^1\Phi_g, ^3\Phi_u$
	$\|2p1,3d2,-\rangle$
$\|2p1,3d2,-\rangle$	−9.017 370

TABLE IV. $^1\Sigma$ eigenvalues and eigenfunctions of the dipole-dipole interaction.

		$^1\Sigma_u^+, {}^3\Sigma_g^+$		
	$E(1)$	$E(2)$	$E(3)$	$E(4)$
	$-72.4232/R^3$	$-8.0075/R^3$	$-0.9814/R^3$	$53.5225/R^3$
	$F(1)$	$F(2)$	$F(3)$	$F(4)$
$\|2s0,3p0,+\rangle$	0.680 734	0.150 824	0.019 979	−0.716 557
$\|2p0,3s0,+\rangle$	0.443 097	0.619 256	0.325 833	0.560 374
$\|2p0,3d0,+\rangle$	0.507 014	−0.354 429	−0.683 198	0.388 017
$\|2p1,3d-1,+,+\rangle$	0.288 448	−0.684 218	0.653 203	0.148 223
		$^1\Sigma_u^+, {}^3\Sigma_g^+$		
	$E(5)$	$E(6)$	$E(7)$	$E(8)$
	$-57.9792/R^3$	$-1.5504/R^3$	$1.5504/R^3$	$57.9792/R^3$
	$F(5)$	$F(6)$	$F(7)$	$F(8)$
$\|2s0,3s0,-\rangle$	−0.629 879	0.321 329	0.321 329	−0.629 879
$\|2s0,3d0,-\rangle$	−0.321 329	−0.629 879	−0.629 879	−0.321 329
$\|2p0,3p0,-\rangle$	−0.582 865	−0.400 335	0.400 335	0.582 865
$\|2p1,3p-1,-,+\rangle$	−0.400 335	0.582 865	−0.582 865	0.400 335
		$^1\Sigma_g^+, {}^3\Sigma_u^+$		
	$E(1)$	$E(2)$	$E(3)$	$E(4)$
	$-53.5225/R^3$	$0.9814/R^3$	$8.0075/R^3$	$72.4232/R^3$
	$F(1)$	$F(2)$	$F(3)$	$F(4)$
$\|2s0,3p0,-\rangle$	−0.716 557	0.019 979	0.150 824	0.680 734
$\|2p0,3s0,-\rangle$	0.560 374	0.325 833	0.619 256	0.443 097
$\|2p0,3d0,-\rangle$	0.388 017	−0.683 198	−0.354 429	0.507 014
$\|2p1,3d-1,-,+\rangle$	0.148 223	0.653 203	−0.684 218	0.288 448
		$^1\Sigma_g^+, {}^3\Sigma_u^+$		
	$E(5)$	$E(6)$	$E(7)$	$E(8)$
	$-73.1673/R^3$	$-2.3741/R^3$	$2.3741/R^3$	$73.1673/R^3$
	$F(5)$	$F(6)$	$F(7)$	$F(8)$
$\|2s0,3s0,+\rangle$	−0.544 367	0.451 292	0.451 292	−0.544 367
$\|2s0,3d0,+\rangle$	−0.451 292	−0.544 367	−0.544 367	−0.451 292
$\|2p0,3p0,+\rangle$	−0.588 119	−0.392 576	0.392 576	0.588 119
$\|2p1,3p-1,+,+\rangle$	−0.392 576	0.588 199	−0.588 119	0.392 576

using the notation

$$\langle nl|r^{la}|n'l'\rangle=\int_0^\infty R^*_{ne}r^{la}R_{nl}dr \tag{A4}$$

for the radial part of the matrix elements. The terms between ( ) are $3j$ Racah coefficients.

The total wave function, including spin, must be antisymmetric with respect to electron exchange; with respect to space, the wave function must be symmetric ($\sigma=+1$) for a singlet state and antisymmetric ($\sigma=-1$) for a triplet state. For the symmetry operator P with respect to inversion through the midpoint of the internuclear axis, if $P\Psi=p\Psi$, $p=+1$ corresponds to an even (g) state, $p=-1$ to an odd (u) state. According to the symmetry rules, the wave function of the unperturbed basis set has to be chosen in the form

$$\begin{aligned}\Psi_0&=|n_1l_1m_1,n_2l_2m_2S\rangle\\&=[2(1+\delta_{n_1n_2}\delta_{l_1l_2}\delta_{m_1m_2})]^{1/2}[\Psi_{n_1l_1m_1}(r_{1a})\Psi_{n_2l_2m_2}(r_{2b})\\&\quad+S\Psi_{n_1l_1m_1}(r_{2b})\Psi_{n_2l_2m_2}(r_{1a})].\end{aligned} \tag{A5}$$

By using the inversion operator I centered on one atom,the operator T that changes the center of the wave function from a to b or vice versa, we get $P=T\cdot I$ (see Ref. [16]) and

TABLE V. Same as Table IV for $^1\Pi$ states.

			$^1\Pi_u, ^3\Pi_g$		
	$E(1)$	$E(2)$	$E(3)$	$E(4)$	$E(5)$
	$-36.7485/R3$	$-4.5658/R3$	$3.0102/R3$	$10.3421/R3$	$46.4155/R3$
	$F(1)$	$F(2)$	$F(3)$	$F(4)$	$F(5)$
$\|2p1,3s0,+\rangle$	−0.436 812	0.190 730	0.765 495	0.286 672	−0.323 502
$\|2p1,3d0,+\rangle$	−0.026 631	−0.860 717	0.155 425	0.409 069	0.258 772
$\|2p0,3d1,+\rangle$	−0.489 801	−0.427 486	−0.165 850	−0.563 265	−0.482 263
$\|2p-1,3d2,+\rangle$	0.277 952	−0.102 276	0.586 769	−0.655 405	0.372 061
$\|2s0,3p1,+\rangle$	0.700 945	−0.172 001	0.134 375	0.060 488	−0.676 296

			$^1\Pi_g, ^3\Pi_u$		
	$E(6)$	$E(7)$	$E(8)$		
	$-45.1870/R3$	0	$45.1870R3$		
	$F(6)$	$F(7)$	$F(8)$		
$\|2s0,3d1,-\rangle$	0.707 107	0.000 000	0.707 107		
$\|2p0,3p1,-\rangle$	−0.593 231	−0.544 201	0.593 231		
$\|2p1,3p0,-\rangle$	−0.384 808	0.838 955	0.384 808		

			$^1\Pi_g, ^3\Pi_u$		
	$E(1)$	$E(2)$	$E(3)$	$E(4)$	$E(5)$
	$-46.4155/R3$	$-10.342/R3$	$-3.0102/R3$	$4.5658/R3$	$36.7485/R3$
	$F(1)$	$F(2)$	$F(3)$	$F(4)$	$F(5)$
$\|2p1,3s0,-\rangle$	−0.323 502	0.286 672	0.765 495	0.190 730	−0.436 812
$\|2p1,3d0,-\rangle$	0.258 772	0.409 069	0.155 425	−0.860 717	−0.026 631
$\|2p0,3d1,-\rangle$	−0.482 263	−0.563 265	−0.165 850	−0.427 486	−0.489 801
$\|2p-1,3d2,-\rangle$	0.372 061	−0.655 405	0.586 769	−0.102 276	0.277 952
$\|2s0,3p1,-\rangle$	−0.676 296	0.060 488	0.134 375	−0.172 001	0.700 945

			$^1\Pi_g, ^3\Pi_u$		
	$E(6)$	$E(7)$	$E(8)$		
	$-31.8639/R3$	0	$31.8639/R3$		
	$F(6)$	$F(7)$	$F(8)$		
$\|2s0,3d1,+\rangle$	0.707 107	0.000 000	0.707 107		
$\|2p0,3p1,+\rangle$	−0.674 518	−0.300 084	0.674 518		
$\|2p1,3p0,+\rangle$	−0.212 191	0.953 913	0.212 191		

$$S=p\sigma(-1)^{l_1+l_2}. \tag{A6}$$

In the case of hydrogen atoms, because of the high degeneracy of the excited levels, the major contribution is due to the dipole-dipole interaction, with $l_a=l_b=1$ leading to R^{-3} terms. We restricted our calculation in this term. The $H^*(n=2)$ states are 4×2 degenerate states; the $H^*(n=3)$ states are 9×2; the $H^*(n=2)+H^*(n=3)$ system represents 8×18 configurations.

Because of $\Lambda=m_1+m_2$ the system can be partitioned into subsystems Σ, Π, Δ, and Φ according to the values 0, ±1, ±2, and ±3 of Λ. Each of these subsystems has singlet and triplet and u and g states. As the V_S matrix elements depend only on the $p\sigma$ product, the $^1\Lambda_g$ and $^3\Lambda_u$ terms (respectively, $^1\Lambda_u$ and $^3\Lambda_g$) are degenerated. For $\Lambda\neq0$, the $^1\Lambda_g$ terms are degenerated with a symmetrical and antisymmetrical superposition of Λ and $-\Lambda$ functions; the results are noted with $\Lambda=|\Lambda|$ for easier reading. For $\Lambda=0$, i.e., Σ states, the symmetry with respect to reflection in the plane containing the internuclear axis, giving $^1\Sigma_u^+$ and $^1\Sigma_u^-$ states, has to be defined.

For the $^1\Sigma_\mu$ states built from $2p1$ and $3d-1$, for in-

TABLE VI. Same as Table V for $^1\Delta$ states.

	$^1\Delta_u, ^3\Delta_g$			
	$E(1)$	$E(2)$	$E(3)$	$E(4)$
	$-13.7783/R3$	$-12.3180/R3$	$3.3006/R3$	$13.7783/R3$
	$F(1)$	$F(2)$	$F(3)$	$F(4)$
$\|2p1,3d1,+\rangle$	0.000 000	0.888 074	0.459 701	0.000 000
$\|2p0,3d2,+\rangle$	0.000 000	−0.459 701	0.888 074	0.000 000
$\|2s0,3d2,-\rangle$	−0.707 107	0.000 000	0.000 000	−0.707.101
$\|2p1,3p2,-\rangle$	0.707 107	0.000 000	0.000 0000	−0.707 107
	$^1\Delta_g, ^3\Delta_u$			
	$E(1)$	$E(2)$	$E(3)$	$E(4)$
	$-24.4054/R3$	$-3.3006/R3$	$12.3180/R3$	$24.4054/R3$
	$F(1)$	$F(2)$	$F(3)$	$F(4)$
$\|2p1,3d1,+\rangle$	0.000 000	0.459 701	0.888 074	0.000 000
$\|2p0,3d2,+\rangle$	0.000 000	0.888 074	−0.459 701	0.000 000
$\|2s0,3d2,-\rangle$	−0.707 107	0.000 000	0.000 000	−0.707 107
$\|2p1,3p2,-\rangle$	0.707 107	0.000 000	0.000 000	−0.707.107

stance, we have to consider the combinations with $2p-1$, $3d1$ giving one $^1\Sigma_u^+$ and one $^1\Sigma_u^-$ term:

$$\Psi(^1\Sigma_u^+)=|2p-1,3d1+,(+)\rangle$$

$$=\frac{1}{\sqrt{2}}(|2p-1,3d1,+\rangle+|2p1,3d-1,+\rangle) \tag{A7}$$

and

$$\Psi(^1\Sigma_u^-)=|2p-1,3d1+,(-)\rangle$$

$$=\frac{1}{\sqrt{2}}(|2p-1,3d1,+\rangle-|2p1,3d-1,+\rangle) \tag{A8}$$

with the similar combinations for the $^1\Sigma_g$ states. The relevant matrices are gathered in Tables I to III. The eigenvalues and eigenfunctions of the doubly excited states of the H_2 molecules are displayed in Tables IV to VI.

[1] S. L. Guberman, J. Chem. Phys. **78**, 1404 (1983).
[2] A. U. Hazi, J. Chem. Phys. **60**, 4358 (1974); Chem. Phys. Lett. **25**, 259 (1974).
[3] M. Leventhal, R. T. Robiscoe, and K. R. Lea, Phys. Rev. **158**, 49 (1967).
[4] M. Misakian and J. C. Zorn, Phys. Rev. A **6**, 2180 (1972).
[5] A. U. Hazi and K. Wiemers, J. Chem. Phys. **66**, 5296 (1977).
[6] J. J. Spezeski, O. K. Kalman, and L. C. McIntyre, Jr., Phys. Rev. A **22**, 1906 (1980).
[7] R. S. Freund, J. A. Schiavone, and D. F. Brader, J. Chem. Phys. **64**, 1122 (1976).
[8] J. A. Schiavone, K. C. Smyth, and R. S. Freund, J. Chem. Phys. **63**, 1043 (1973).
[9] M. Glass-Maujean, J. Phys. B **11**, 431 (1978); Comments At. Mol. Phys. **7**, 83 (1977).
[10] M. Glass-Maujean, J. Chem. Phys. **85**, 4830 (1986).
[11] S. Arai, T. Yoshimi, M. Morita, K. Hironaka, T. Yoshida, H. Koizumi, K. Shinsaka, Y. Hatano, A. Yagishita, and K. Ito, Z. Phys. D **4**, 65 (1986).
[12] M. Glass-Maujean, J. Chem. Phys. **89**, 2839 (1988).
[13] M. Glass-Maujean, J. Breton, B. Thièblemont, and K. Ito, Phys. Rev. A **32**, 947 (1985).
[14] M. A. Bethe and E. E. Salpeter, *Quantum Mechanics of One and Two Electron Atoms* (Springer, Berlin, 1957).
[15] G. Herzberg, *Spectra of Diatomic Molecules* (Van Nostrand Reinhold, New York, 1950).
[16] T. L. Stephens and A. Dalgarno, Mol. Phys. **28**, 1049 (1974).
[17] P. R. Fontana, Phys. Rev. **123**, 1865 (1961); **123**, 1871 (1961).
[18] W. Kolos, Int. J. Quantum Chem. **1**, 169 (1967).
[19] S. I. Nikitin, V. N. Ostrovskii, and N. V. Prudov, Zh. Éksp. Teor. Fiz. **91**, 1262 (1986) [Sov. Phys. JETP **64**, 745 (1986)].